Mimicking sarcolemmal damage *in vitro*: a contractile 3D model of skeletal muscle for drug testing in Duchenne muscular dystrophy

Biofabrication

PAPER

Mimicking sarcolemmal damage *in vitro*: a contractile 3D model of skeletal muscle for drug testing in Duchenne muscular dystrophy

Ainoa Tejedera-Villafranca[1], **Marisol Montolio**[2,3], **Javier Ramón-Azcón**[1,4,*] and **Juan M Fernández-Costa**[1,*]

[1] Institute for Bioengineering of Catalonia (IBEC), The Barcelona Institute of Science and Technology (BIST), C/Baldiri Reixac 10-12, E08028 Barcelona, Spain
[2] Duchenne Parent Project España, E28032 Madrid, Spain
[3] Department of Cell Biology, Physiology and Immunology, Faculty of Biology, University of Barcelona, E08027 Barcelona, Spain
[4] Institució Catalana de Reserca i Estudis Avançats (ICREA), Passeig de Lluís Companys, 23, E08010 Barcelona, Spain
[*] Authors to whom any correspondence should be addressed.

E-mail: jramon@ibecbarcelona.eu and jfernandez@ibecbarcelona.eu

Keywords: Duchenne muscular dystrophy, sarcolemmal damage, skeletal muscle, disease modeling, tissue engineering, 3D cell culture, drug testing

Supplementary material for this article is available online

OPEN ACCESS

RECEIVED
22 June 2023

REVISED
28 August 2023

ACCEPTED FOR PUBLICATION
19 September 2023

PUBLISHED
27 September 2023

Abstract

Duchenne muscular dystrophy (DMD) is the most prevalent neuromuscular disease diagnosed in childhood. It is a progressive and wasting disease, characterized by a degeneration of skeletal and cardiac muscles caused by the lack of dystrophin protein. The absence of this crucial structural protein leads to sarcolemmal fragility, resulting in muscle fiber damage during contraction. Despite ongoing efforts, there is no cure available for DMD patients. One of the primary challenges is the limited efficacy of current preclinical tools, which fail in modeling the biological complexity of the disease. Human-based three-dimensional (3D) cell culture methods appear as a novel approach to accelerate preclinical research by enhancing the reproduction of pathophysiological processes in skeletal muscle. In this work, we developed a patient-derived functional 3D skeletal muscle model of DMD that reproduces the sarcolemmal damage found in the native DMD muscle. These bioengineered skeletal muscle tissues exhibit contractile functionality, as they responded to electrical pulse stimulation. Sustained contractile regimes induced the loss of myotube integrity, mirroring the pathological myotube breakdown inherent in DMD due to sarcolemmal instability. Moreover, damaged DMD tissues showed disease functional phenotypes, such as tetanic fatigue. We also evaluated the therapeutic effect of utrophin upregulator drug candidates on the functionality of the skeletal muscle tissues, thus providing deeper insight into the real impact of these treatments. Overall, our findings underscore the potential of bioengineered 3D skeletal muscle technology to advance DMD research and facilitate the development of novel therapies for DMD and related neuromuscular disorders.

1. Introduction

Duchenne muscular dystrophy (DMD; OMIM: 310200) is a severe and degenerative pediatric muscular dystrophy. Affecting more than 1 in 5000 newborn males, it is the most prevalent neuromuscular disease diagnosed during childhood [1]. DMD is an X-linked recessive genetic disorder caused by mutations in the dystrophin gene (*DMD;* Gene ID: 1756), consisting of 79 exons and encoding the dystrophin protein. Several types of mutations in the DMD gene can cause the disease, leading to a frameshift or causing abnormal domain function of dystrophin [2]. Even though DMD is mainly manifested as a degenerative and necrotic muscle disease, it cannot be understood by only one mechanism [3]. However, sarcolemma weakening is considered the primary consequence of dystrophin deficiency. Dystrophin bridges the inner cytoskeleton with the sarcolemma and the basal lamina of the extracellular matrix

(ECM), thus forming the dystrophin-glycoprotein complex (DGC) [4]. In DMD, the lack of dystrophin disrupts the DGC, which causes the loss of interaction between F-actin and the ECM, and the fragility of the muscle membrane increases [5]. This leads to sarcolemma weakening and, consequently, muscle fiber damage developed during muscle contraction [6]. The degenerated muscle is regenerated during the early phase of the disease. However, fatty and fibrotic tissue finally replaces damaged muscle cells in later phases [7].

Consequently, DMD patients suffer from progressive degeneration of skeletal and cardiac muscles. This event causes critical muscle wasting, inability to walk, cardiac or respiratory failure, and death before 30 years [8]. To date, no long-term cure is available for patients, even though several molecules are in drug development. However, the overall success rate of drugs remains low, primarily due to the drug's high toxicity or low efficacy in humans when it enters clinical phases [9]. This is especially dramatic in rare diseases such as DMD, which are intrinsically very heterogeneous [10].

The emerging therapies for DMD mainly pursue two strategies: targeting the progressive dystrophic pathology, such as enhancing muscle growth and repair, or restoring dystrophin or dystrophin surrogate molecules [11, 12]. Regarding the last approach, several promising strategies have been explored. These include viral gene therapies, antisense oligonucleotides (ASOs) for exon skipping, utrophin up-regulation, and, more recently, CRIPSR-Cas9-mediated gene editing. To date, the approved ASOs treatments have achieved only minimal restoration of dystrophin levels due to limited uptake by skeletal muscle and heart tissues [13]. Therefore, ongoing research is directed towards refining delivery mechanisms [14, 15]. On the other hand, CRIPSR-Cas9-mediated genome editing has shown substantial preclinical promise for potential translation into clinical applications [16]. The US Food and Drug Administration has recently granted approval the first gene therapy for specific DMD patients, though its impact on muscle function is moderate [17].

Other treatments, such as utrophin up-regulators, are positioned to play an important role within comprehensive treatment approaches integrated with genetic and cell therapies. These drugs would be applicable to all patients, irrespective of their genetic mutation. The small molecule Ezutromid (SMTC1100) was the first orally bioavailable utrophin modulator. Despite promising preclinical results, a Phase 2 clinical study (NCT02858362) failed to reach the proposed endpoints [18]. Similarly, Halofuginone, an antifibrotic small molecule [19], was proposed as a utrophin regulator [20, 21]. Nevertheless, Phase 2 clinical studies were unsuccessfully terminated (NCT02525302, NCT01978366).

Traditional cell culture and animal models, the gold standard models of preclinical drug development, show numerous limitations, restricting drugs from reaching the patients [22–24]. On the one hand, conventional cell cultures do not mimic the complexity of biological tissue architectures, as cells are cultured in two-dimensional (2D) monolayers. Consequently, they lack the surrounding three-dimensional (3D) environment of actual tissues. This includes the cell–cell and cell–matrix interactions that involve the 3D ECM [22]. Specifically in skeletal muscle modeling, 2D cell culture of myogenic precursors fails in the recapitulation of the organized structure of myotubes. This is essential to achieve muscle contractile function, which is crucial for reproducing some disease features. For instance, standard 2D cell culture fails to simulate sarcolemmal damage of DMD. On the other hand, animal models often fail when extrapolating data to human conditions, probably due to species-specific differences. Moreover, their use raises several ethical concerns and a high cost and low throughput [23]. All these limitations evidence the need for new approaches to accelerate preclinical research.

Tissue engineering arises as a promising alternative to traditional skeletal muscle disease models [25]. Human-based 3D cell culture methods aim to mimic the complex architecture of skeletal muscle. This is achieved by culturing the cells using specific biofabrication techniques on a biomaterial scaffold. By providing structural support and integrity for the tissue, the reproduction of pathophysiological processes of skeletal muscle is improved [25, 26]. As a result, functional bioengineered 3D skeletal muscle cell cultures are achieved, as they can be electrically stimulated and respond by contracting [27–29].

In this work, we developed a contractile patient-derived 3D skeletal muscle model of DMD that reproduces the damage of the sarcolemma found in the native muscle of DMD patients. The membrane disruption was induced by the electrical stimulation of skeletal muscle tissues, which responded by contracting. This was essential to generate sarcolemmal damage in DMD tissues, as it was only produced after specific contractile regimens. In consequence, DMD tissues showed functional fatigue-like phenotypes. Additionally, this 3D skeletal muscle *in vitro* model evaluated the effect of utrophin upregulator drug candidates, thus identifying the most effective molecules. Overall, these findings demonstrate that patient-derived bioengineered 3D skeletal muscle tissues are a valuable *in vitro* tool for preclinical research for DMD. They can reproduce physiological functions often limited in traditional cell culture methods, making them more effective in evaluating therapeutic compounds. This is highly relevant to accelerate drug development for DMD and other muscular dystrophies.

2. Experimental section

2.1. Cell culture

Immortalized human muscle precursor cells from unaffected controls (Control 1, clone D6; Control 2, clone E4; Control 3, clone A42) and DMD patients (DMD1 clone G8; DMD 2, clone G82; DMD4, clone B42) were kindly provided by Dr Bénédicte Chazaud (Institut NeuroMyoGène, Lyon, France) [30]. Cells were cultured in growth medium (skeletal muscle basal medium (PromoCell GmbH), skeletal muscle supplemental mix (PromoCell GmbH), 10% fetal bovine serum (Gibco™), 100 U ml^{-1} penicillin and 100 μg ml^{-1} streptomycin (Gibco™), at 37 ℃ in a humidified atmosphere containing 5% CO_2.

2.2. Fabrication of patient-derived 3D skeletal muscle tissues

Human 3D skeletal muscle tissues were fabricated using polydimethylsiloxane (PDMS; Sylgard 184 silicone elastomer kit, Dow Corning;) casting molds as previously described [31]. Briefly, the casting molds design consists of a rectangular-shaped pool, where the cells/hydrogel solution is seeded, and two vertical, flexible PDMS pillars. PDMS casting mold were prepared for muscle cell culture by first cleaning them by sonication in water with detergent, 2-propanol, and mili-Q water and sterilized with UV light for 15 min. It was followed by 1 h treatment with 1% Pluronic® F-127 (Sigma-Aldrich) solution in cold phosphate-buffered saline (PBS) (100 μl $well^{-1}$) at 4 ℃.

Cells were encapsulated at 2.5×10^7 cells ml^{-1} in a cell/hydrogel mixture of 30% v/v Corning® Matrigel® Growth Factor Reduced Basement Membrane Matrix (Corning®), 2 units ml^{-1} of thrombin from human plasma (Sigma-Aldrich) and 4 mg ml^{-1} of fibrinogen from human plasma (50% v/v) (Sigma-Aldrich). The mix was pipetted within each PDMS casting mold using cold tips to avoid premature polymerization.

The cell/hydrogel mixture was polymerized for 30 min at 37 ℃, followed by incubation in growth medium containing 1 mg ml^{-1} of 6-aminocaproic acid (ACA) (Sigma-Aldrich). ACA works as an anti-fibrinolytic, which avoids fibrin depolymerization. They were kept in growth media for two days and then switched to differentiation medium (Dulbecco's Modified Eagle Medium, high glucose, GlutaMAX™ Supplement (Gibco™), containing 1% KnockOut™ Serum replacement (Gibco™), 1% Insulin-Transferrin-Selenium-Ethanolamine (Gibco™) and 1% Penicillin-Streptomycin-Glutamine (Gibco™)) containing 1 mg ml^{-1} of ACA for seven days. Half of the volume of differentiation medium was replaced every two days.

2.3. Utrophin up-regulators treatment

Ezutromid, Halofuginone and the SOM utrophin up-regulator (EU Patent No. EP22382147) were kindly provided by SOM Innovation Biotech, S.A. The screening and study of the selected candidate SOM utrophin up-regulator will be published elsewhere. For drug administration, after five days of differentiation, the medium was replaced by differentiation medium with the drugs at the desired concentration (0.01–10 μM) in 0.01% DMSO. The treatment was kept for 48 h.

2.4. Electrical pulse stimulation (EPS)

Human 3D skeletal muscle tissues were electrically stimulated after seven days of differentiation to induce muscle contraction. A custom-made device consisting of a 12-well plate with two graphite electrodes per well located on the lid was used to perform the EPS. PDMS casting molds were placed on a 12-well plate with fresh differentiation medium. The plate was placed on a Zeiss Axio Observer Z1/7 outfitted with the XL S1 cell incubator at 37 ℃ and 5% CO_2. The device was connected to a pulse generator (Multifunction Generator WF1974, NF Corporation), and tissues were stimulated with electrical square-wave pulses of 1 V mm^{-1}, 1 ms of pulse width, and frequencies varying from 1 to 50 Hz.

2.5. Video analysis and force measurement

The force that the 3D skeletal muscle tissue produced against the pillars when they contracted in response to the EPS was measured using the displacement of the top part of the pillars. Top-view brightfield videos of the pillars for force measurement or fluorescent videos of the sample for calcium analysis were taken during EPS with a ZEISS Axio Observer Z1/7 microscope. The diameter and location of each tissue on the y-axis of the pillar was estimated during the assay using brightfield imaging of the sample. The focal planes that corresponded to the tissue's position were recorded.

Fiji image processing package, a distribution of Image Schindelin *et al* [32, 33], was used to measure the pillar's displacement and calcium fluorescence. For force measurement, the edges of the structure were detected using a Sobel edge detector, followed by the measurement of the pixel displacement of the border along a hand-selected perpendicular straight line [34].

Euler–Bernoulli's beam bending equation was used to calculate the forces exerted from the 3D skeletal muscle tissues using a custom-made Python script, following the equation $F = \frac{6\pi ED^4}{64a^2(3L-a)}y(a)$ where: F is the applied force; E is the Young's modulus of the PDMS (1.6 MPa); D is the diameter of the post; a is the height from which the tissue exerts the force; L is the height of the post, from where the movement of the post is recorded; and $y(a)$ is the displacement of the post [34]. The resulting forces were normalized by the cross-sectional area of each sample, $sF = \frac{F}{\pi R^2}$, where sF is the normalized specific force and R the radius of the tissue [28].

2.6. Evans blue dye (EBD) muscle damage assay

Myotube damage was evaluated by EBD uptake assay after EPS of human 3D skeletal muscle tissues. Specifically, PDMS casting molds were placed on a 12-well plate with fresh differentiation medium containing 0.25 mg ml^{-1} of EBD (Sigma-Aldrich) [35]. Next, tissues were stimulated as described in EPS section. After EPS, tissues were incubated at 37 ℃ for 1 h, followed by three washes of 5 min with PBS. Samples were fixed, cryosectioned and counterstained for nuclei and cytoskeleton using 4′,6-diamidino-2-phenylindole (DAPI) and A488-phalloidin.

2.7. Cryosectioning

Human 3D skeletal muscle tissues were fixed in 10% formalin solution (approx. 4% formaldehyde) (Sigma-Aldrich) for 30 min at room temperature (RT) and washed three times with PBS for 5 min. Samples were removed from the PDMS platform and placed on 30% sucrose solution in PBS for 48 h at 4 ℃ in agitation. They were frozen by embedding them in optimal cutting temperature compound (PolyFreeze, Sigma-Aldrich) within a disposable plastic Cryomold® (VWR) using a batch of isopentane chilled by liquid nitrogen. Samples were stored at −20 ℃ until sectioning. They were sectioned with a cryostat (Leica CM1900) to obtain transverse sections at a thickness of 20 μm that were placed on SuperFrost Plus™ Adhesion slides (Fisher Scientific) and stored at −20 ℃ until staining was performed. Before staining, slides containing tissue sections were encircled with a PAP pen (ImmEdge™, Vector laboratories).

2.8. Immunohistochemistry and fluorescent methods

The fluorescent calcium binding dye Fluo-8 AM (Abcam) was used to evaluate intracellular calcium influx according to the manufacturer's instructions. Briefly, samples were washed with PBS and incubated with Fluo-8 loading solution for 1 h at 37 ℃ before the EPS. The fluorescent signal was recorded during EPS and analyzed (see section 2.5).

For immunohistochemistry and other fluorescent stainings, cryosections or whole-mount samples were permeabilized with PBS-T (0.1% Triton-X (Sigma-Aldrich) in PBS) for 10 or 15 min, followed by incubation with blocking buffer (0.3% Triton-X, 3% donkey serum (Sigma-Aldrich) in PBS) for 30 min or 2 h at RT. Next, samples were incubated with the primary antibody (supplementary table 1) in blocking buffer at 4 ℃ overnight. After 3 PBS-T washes of 5 min, the samples were incubated for 45 min or 2 h at RT with fluorophore-conjugated secondary antibody (supplementary table 1) or phalloidin. After 3 PBS-T washes of 5 min, whole-mount samples were incubated for 30 min with DAPI (Life Technologies). Samples were washed for 5 min with PBS before they were mounted with VECTASHIELD Plus Mounting Medium with DAPI (Palex) or Fluoromount-G™ Mounting Medium (Thermo Fisher). Transparent enamel was used to seal the edges of coverslips.

2.9. Imaging and image analysis

Brightfield images were taken with ZEISS Axio Observer Z1/7 microscope. Fluorescence images were taken with a ZEISS LSM800 confocal laser scanning microscope. Images were analyzed using the Fiji image processing package [32]. For EBD uptake quantification, binary images of F-actin were used for myotubes identification. Analyze particles tool selected objects of more than 30 μm. Next, the mean gray values of each myotube in the channel of interest were calculated. For utrophin signal quantification, the mean gray values of each image were measured. For myotube diameter measurements, segmentation was performed using utrophin signal with Cellpose 2 software [36] and ImageJ plugin LabelsToRois [37] to measure Feret diameter.

2.10. Theoretical simulations

COMSOL Multiphysics® software was used to perform theoretical simulations. The solid mechanics module was used to study the pillars displacement of the PDMS casting mold simulating the force load to the pillars.

2.11. Statistical analysis

The comparisons between groups were performed using Prism 8 software (GraphPad). Statistical test outcomes are reported as mean ± SEM. Pairs of samples were compared using a two-tailed student t-test ($\alpha = 0.05$), applying Welch's correction if needed. Multiple comparisons were analyzed by one-way or repeated measures two-way ANOVA followed by Tukey's range multiple comparisons test. Differences between groups were considered significant when $P < 0.05$ ($*P < 0.05$; $**P < 0.01$; $***P < 0.001$).

3. Results

3.1. Fabrication and histological characterization of patient-derived 3D skeletal muscle tissues

To fabricate human 3D skeletal muscle tissues using both unaffected controls (CNT) and DMD patient-derived cells, we used hydrogel molding technique. PDMS casting molds consisting of a square well containing two pillars (figure 1(a)) were used to encapsulate immortalized human muscle precursor cells in a matrix of fibrin and Matrigel® (figure 1(b)). Hydrogel compaction started during the first hours after encapsulation, and tissues were completely detached from the PDMS surface after 1 d (figures 1(c) and S1(a)). After two days in growth conditions, samples were

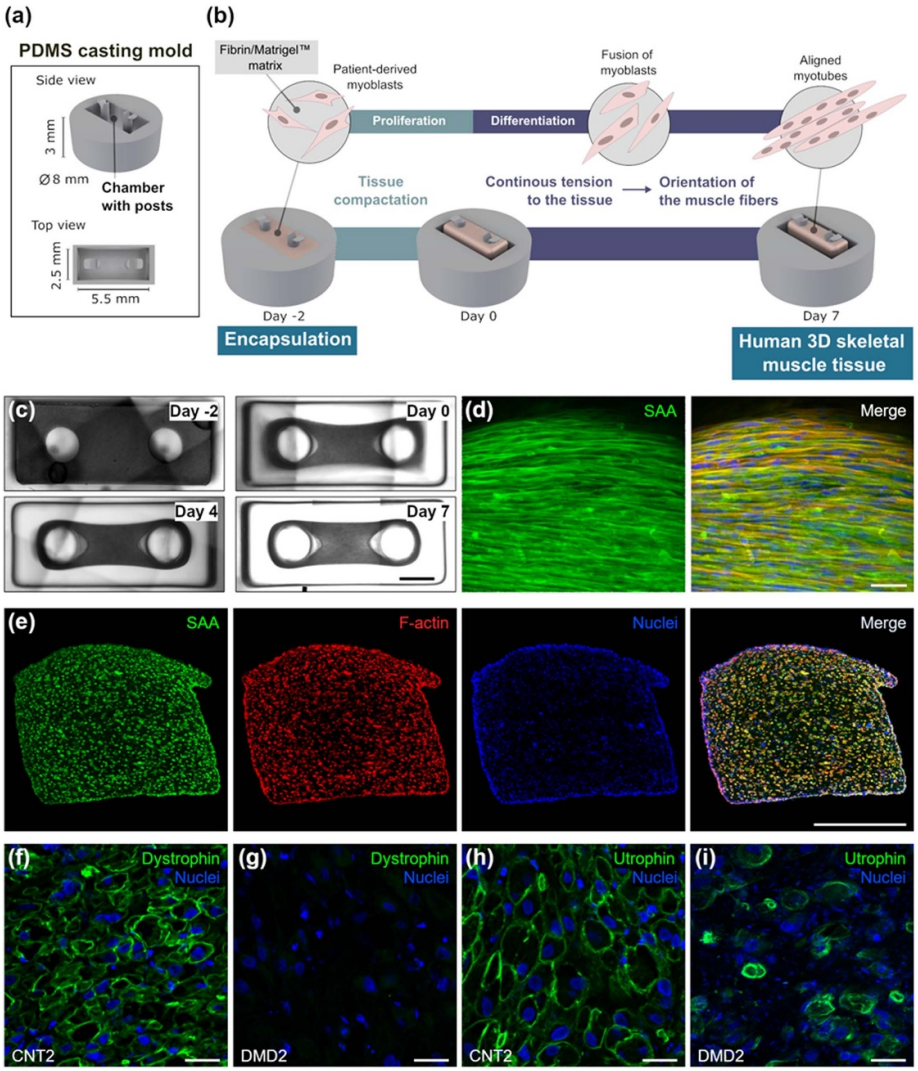

Figure 1. Human 3D skeletal muscle tissues fabrication. (a) Schematic of the encapsulation PDMS casting mold. (b) Schematic of encapsulation process and experimental timeline. (c) Representative top-view brightfield images of CNT tissue compaction at different time points. Scale bar = 1 mm. (d) Representative confocal images of CNT tissue after seven days of differentiation stained for sarcomeric α-actinin (SAA, green), F-actin (red) and nuclei (blue). Scale bar = 50 μm. (e) Representative confocal images of transversal cross-sections of a tissue stained for SAA (green), F-actin (red) and nuclei (blue). Scale bar = 500 μm. (f)–(i) Representative confocal images of transversal cross-sections of CNT (f), (h) and DMD tissues (g), (i) stained for dystrophin (green) (f)–(g) or utrophin (green) (h)–(i) and nuclei (blue). Scale bar = 25 μm.

changed to differentiation medium, which was kept for seven days (figure 1(b)). Within one week of differentiation, 3D skeletal muscle tissues formed multinucleated and aligned myotubes, as evidenced by sarcomeric α-actinin (SAA) immunofluorescence staining (figures 1(d) and S1(b)).

In order to further characterize CNT and DMD skeletal muscle tissues, we conducted immunostaining on transverse tissue cross-sections for SAA (figures 1(a) and S2). Differentiated myotubes were uniformly present in most of the cross-sectional area, indicating effective media diffusion throughout the tissue. Furthermore, only CNT samples expressed dystrophin (figures 1(f) and (g)). Utrophin could be detected in both CNT and DMD tissues by immunostaining (figures 1(h) and (i)), which was necessary for the evaluation of therapeutic compounds that target its upregulation.

3.2. Functional analysis of DMD 3D skeletal muscle tissues

To explore the presence of functional phenotypes in the DMD 3D tissues, their contractile was evaluated. Briefly, 3D skeletal muscle tissues were electrically stimulated after seven days of differentiation to induce muscle contraction. This caused the deformation of the PDMS posts, which was used as an indirect measurement of the tissue's force (figure 2(a)). The deformation of the pillars was estimated using COMSOL Multiphysics® software (figure S3), simulating a range of forces applied by the sample from 5 μN to 50 μN.

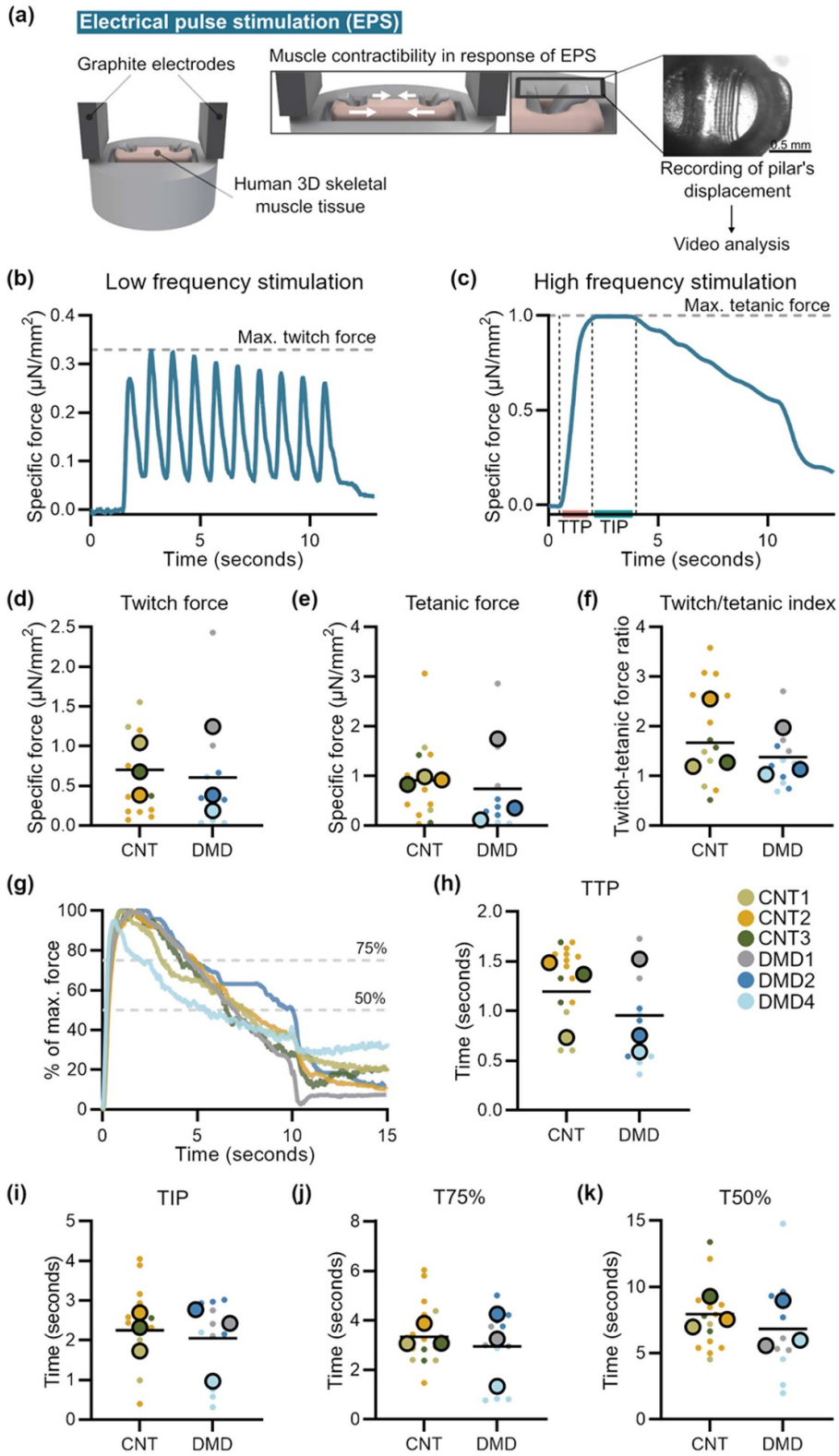

Figure 2. Human 3D skeletal muscle tissues respond to electrical pulse stimulation (EPS). (a) Schematic of the EPS. (b) and (c) Representative twitch (b) and tetanic (c) specific force measurements in response to low (1 Hz, b) and high (50 Hz, c) frequency electrical stimulations. TTP = time to peak, TIP = time in peak. (d)–(f) Maximum twitch (d) and tetanic (e) specific forces, and twitch/tetanic force ratio (f) performed by CNT1-3 and DMD1-2,4 tissues during 1 and 50 Hz stimulation. (g) Representative force during 50 Hz stimulation for 10 s normalized to the maximum peak force performed by CNT1-3 and DMD1-2,4 tissues. (h)–(k) Time to peak (h), time in peak (i) and time to relaxation to the 75% (T75%) (j) and 50% (T50%) (k) of the maximum force performed by CNT1-3 and DMD1-2,4 tissues during 50 Hz stimulation for 10 s. $N = 3$–9 tissues per cell line. Significance was determined using two-tailed student t-test to compare differences between the groups. Statistical test outcomes are reported as mean ± SEM.

After seven days of differentiation, CNT and DMD 3D skeletal muscle tissues were competent to produce contractions in response to electrical stimuli. At low EPS frequencies, tissues showed twitch contraction dynamics (figure 2(b) and supplementary video 1). On the other hand, tetanic-like dynamics were observed in response to high EPS frequencies (figure 2(c) and supplementary video 1). To evaluate the differences in the contractile dynamics between CNT and DMD samples, we measured the maximum twitch and tetanic forces and the ratio between these forces (twitch/tetanic index). The forces were normalized by the cross-sectional area of each tissue. Moreover, we used tetanic dynamics to assess the time needed to reach the peak (time to peak, TTP), the duration of the contraction maintained in the maximum force (time in peak, TIP), the time that the force decreased to the 75% of the total force (T75%) and the 50% of total force (T50%).

Using this strategy, we examined the contractile response of 3D skeletal muscle tissues fabricated from three CNT and three DMD cell lines. In general, none of the investigated parameters revealed disease-specific functional phenotypes. The 3D tissues displayed variable maximum forces and twitch/tetanic index across the different cell lines (figures 2(d)–(f)). However, this variability was particularly pronounced in the DMD cell lines. Specifically, DMD2 and DMD4 tissues exhibited lower contractile forces, especially during tetanic dynamics, compared to all CNT 3D tissues, while DMD1 exhibited higher maximum forces than CNT samples. The twitch/tetanic index ranged from 1 in CNT1,3 and DMD2,4–2-2.5 in CNT2 and DMD1.

Focusing on tetanic responses, the stimulation of the tissues with high frequency (50 Hz) for 10 s did not report relevant differences between CNT and DMD samples (figures 2(g)–(k)). TTP was similar in CNT1 and DMD2,4 samples but increased for CNT2,3 and DMD1 tissues (figure 2(h)). However, we could observe cell line-specific dynamics, such as tetanic fatigue in DMD1 tissues, that performed lower TIP and T75% (figures 2(i) and (j)). Finally, all samples reached half of the relaxation before the EPS was stopped (<10 s) (figures 2(g) and (k)).

Furthermore, we evaluated intracellular calcium transient responses to EPS. Through the application of a frequency range spanning, we observed twitch (figure S4(a)), unfused tetanic (figures S4(b) and (c)) and complete tetanic (figure S4(d)) responses. Notably, we identified a consistent trend of lower calcium transients in DMD2 tissues compared to CNT2 tissues during twitch or unfused tetanic responses (figures S4(a)–(c) and (e)). In the case of complete tetanic dynamics, some of these DMD2 samples exhibited closer calcium levels to CNT2 samples (figures S4(d) and (f)). This event increased the twitch/tetanic index of DMD2 samples (figure S4(d)). However, these samples failed to sustain their peak (figure S4(d)). Consequently, this resulted in lower TIP and T75%. Nonetheless, we identified that specific DMD2 samples ($n = 2$ from a total of 8) performed similar dynamics to CNT2, and the overall significance of the results was diminished.

3.3. Sarcolemmal damage is induced in DMD 3D skeletal muscle tissues after contraction regimes and causes tetanic fatigue-like phenotypes

Dystrophin plays an essential role in protecting muscle fibers from damage developed during muscle contraction [6]. Therefore, DMD sarcolemmal damage is dependent on muscle contraction. To explore if sarcolemmal damage was induced in DMD 3D skeletal muscle tissues after EPS, we used EBD assay. EBD strongly binds to extracellular proteins like albumin [38] and has been used as an *in vivo* marker of myofiber damage [39].

We selected CNT2 and DMD2 3D tissues to study muscle damage induction because of their similar performance in key functional parameters (twitch force, TIP, T75% and T50%) (figure 2). However, these two cell lines also displayed distinct behaviors regarding tetanic force, twitch/tetanic index and TTP (figure 2). This characteristic is particularly valuable to both examine the changes of specific indices resulting from sarcolemmal damage, and explore the potential improvement of different parameters following therapeutic strategies.

The 3D skeletal muscle tissues were exposed to EPS regimens ranging from 0 to 30 min at 1 Hz of frequency. They were incubated in medium containing EBD when EPS was applied and incubated for 1 h. Transversal sections were obtained to analyze the presence of EBD uptake. The levels of EBD's fluorescence signal in each myotube were analyzed using confocal microscopy images (figure S5). The results revealed that DMD2 tissues did not show sarcolemmal damage without or with short (5 min) twitch contractile activity (figure S5). However, DMD2 samples exhibit a significant increase in EBD uptake after 15 min of twitch contractions in comparison with CNT2 tissues (figures 3(a) and (b)). These results indicate that sarcolemmal damage is induced in DMD 3D skeletal muscle tissues by using prolonged twitch contractile dynamics.

To assess the functional consequences of the sarcolemmal damage in DMD 3D tissues, we evaluated the contractile dynamics before and 24 h after the damage induction (figure 3(c)). They maintained similar twitch force before the damage, and, after 24 h, it increased, although non-significantly. As expected, CNT tissues showed higher maximum tetanic forces than DMD. After damage, some samples also experienced an increase in the tetanic peak value. The twitch/tetanic index did not experience any change. This event of increased maximum forces could be explained by the improvement in the muscle differentiation status following an additional day in culture.

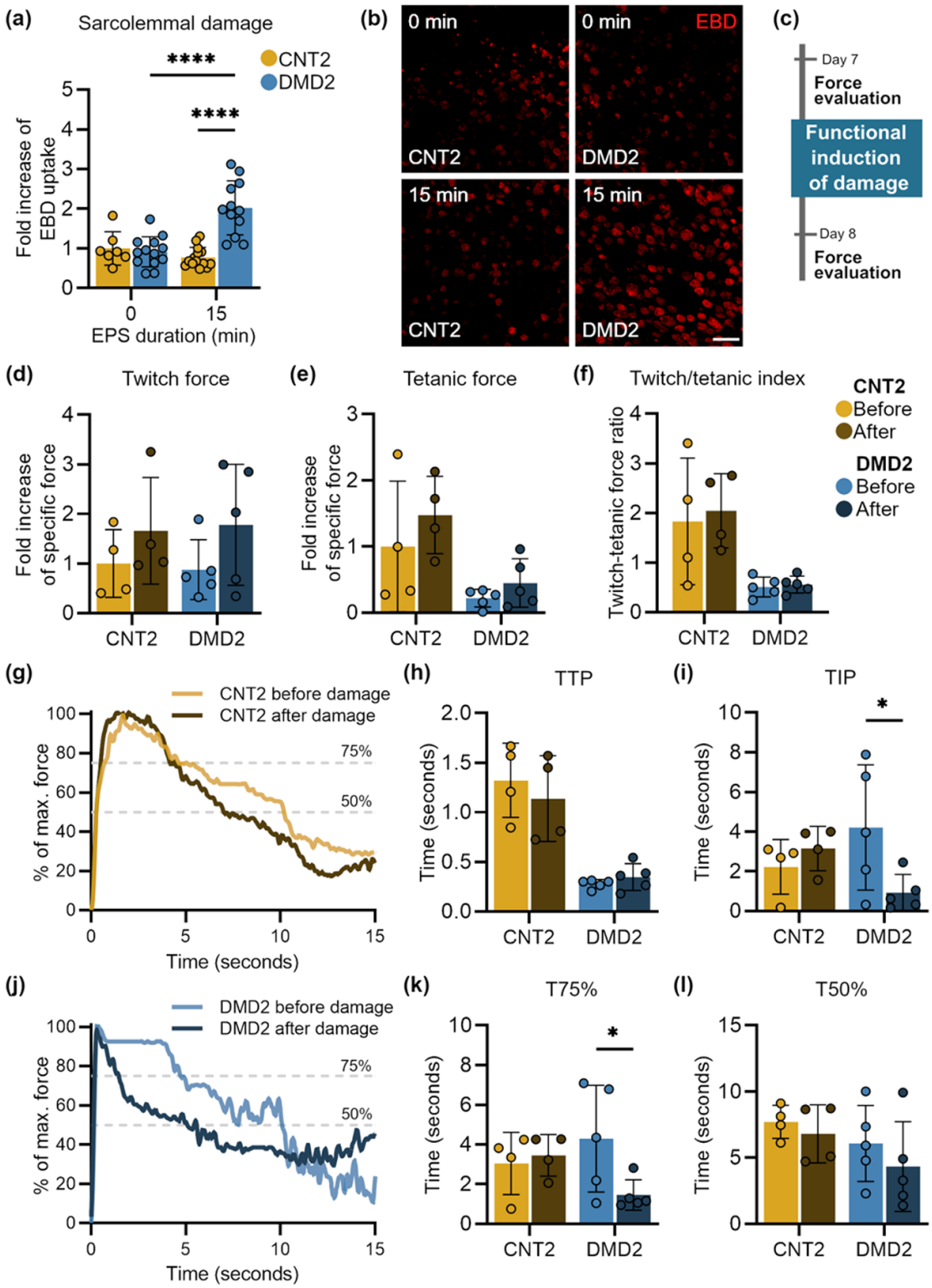

Figure 3. DMD human 3D skeletal muscle tissues reproduce sarcolemmal damage after electrical pulse stimulation (EPS). (a) Comparison of Evans blue dye (EBD) uptake (expressed as the fold increase of the mean gray value of EBD per myotube compared with non-stimulated CNT2 levels) of CNT2 and DMD2 tissues without stimulation or after 15 min of 1 Hz EPS. (b) Representative confocal images of transversal cross-sections of CNT2 and DMD2 tissues without stimulation or after 15 min of EPS performing EBD assay (EBD in red). Scale bar = 50 μm. (c) Schematic of the experimental flow of the functional induction of damage. (d)–(f) Fold increase of maximum twitch (d) and tetanic (e) specific forces and twitch/tetanic force ratio (f) compared with non-stimulated CNT2 performed by CNT2 and DMD2 tissues before or after 24 h of the damage EPS during 1 and 50 Hz stimulation. (g) and (j) Representative force during 50 Hz stimulation for 10 s normalized to the maximum peak force performed by CNT2 (g) and DMD2 (j) before or after 24 h of the damage EPS. (h)–(i), (k)–(l) Time to peak (TTP) (h), time in peak (TIP) (i), time to relaxation to the 75% (T75%) (k) and 50% (T50%) (l) of the maximum force performed during 50 Hz stimulation for 10 s by CNT2 and DMD2 before or after 24 h of the damage EPS. $N = 4$–5 tissues per group. Significance was determined using two-way repeated measures ANOVA followed by Tukey's range multiple comparisons test to compare differences between the groups. Statistical test outcomes are reported as mean ± SEM ($*p < 0.05$; $****p < 0.0001$).

Focusing on tetanic dynamics, after 24 h of the induction of sarcolemmal damage, we observed that DMD muscle tissues showed a tetanic fatigue-like phenotype (figures 3(g) and (j)). Damaged DMD samples failed to sustain the contraction on the peak, which caused a decreased in TIP and T75% values (figures 3(i) and (k)). These findings suggest that sarcolemmal damage induces functional phenotypes in DMD samples by compromising their performance during high-frequency EPS, leading to tetanic fatigue.

3.4. Utrophin upregulator treatment improves DMD functional performances

Utrophin is a structural and functional paralogue of dystrophin protein that could play a role as a dystrophin surrogate. Several strategies to overexpress utrophin are being explored, and some small molecules have been identified to induce its upregulation [18]. Ezutromid and Halofuginone are some examples of small molecules that have been reported to increase utrophin expression and enhance muscle function in *in vitro* DMD models [20, 40]. To assess the response of DMD 3D skeletal muscle tissues to Ezutromid and Halofuginone treatments, we treated DMD2 samples from day 5 to day 7 of differentiation using concentrations ranging from 3 to 0.01 μM, according to previous results. On day 7, samples were electrically stimulated, and we obtained transversal sections to analyze utrophin expression. We observed that utrophin signaling significantly increased after the treatment with Ezutromid 3 μM (figure 4(a)). However, DMD tissues treated with Ezutromid 3 μM and Halofuginone 1 and 0.1 μM were not competent to produce contractions (data not shown). Moreover, treatment with Ezutromid 1 μM and Halofuginone 0.01 μM decreased notably muscle contractile function (data not shown). Myotube size was not decreased after treatment with Ezutromid. However, we found a significant reduction in myotube diameter after treatment with Halofuginone 1 μM (figure S6). This suggests that Halofuginone treatment induced an atrophic effect, possibly due to a toxic influence on the 3D skeletal muscle tissues, which reduced their functionality. Altogether, these results suggest that both Ezutromid and Halofuginone may not be optimal candidates to target the increase of utrophin expression.

We proceeded to explore the effect of other novel treatments that modulate utrophin expression. DMD2 3D skeletal muscle tissues were treated with a small molecule identified by SOM Innovation Biotech S.A. as a potential utrophin upregulator and confirmed in 2D cell culture (screening and selection of the candidate will be published elsewhere). DMD tissues treated with SOM utrophin upregulator showed nearly a three-fold increase of utrophin signal (figures 4(b) and (c)). Force evaluation revealed an increase of both twitch and tetanic maximum forces, as well as twitch/tetanic index (figures 4(d)–(f)). Maximum forces were higher than those performed by CNT2 samples, and its ratio achieved similar CNT2 values. This force increase did not correlate with an increase in myotube diameter (figure S6). Focusing on the tetanic response, TTP was enhanced compared to tissues treated with DMSO, eventually reaching values like those observed in CNT2 responses. Finally, TIP and T75% increase in DMSO and SOM samples, doubling the times performed by CNT2 and non-treated DMD2 samples.

Next, we evaluated the potential of SOM utrophin upregulator to provide protection against sarcolemmal damage in DMD 3D skeletal muscle tissues. To accomplish this, DMD tissues were treated with SOM utrophin upregulator for two days and exposed to a 15 min twitch contractile cycle. The analysis of sarcolemmal damage revealed no significant decrease in EBD uptake in DMD 3D skeletal muscle tissues following SOM treatment. These findings suggest that the observed increase of utrophin levels after treatment with SOM utrophin upregulator may not shield DMD 3D tissues from contraction-induced sarcolemmal damage. Therefore, SOM treatment may enhance DMD functional contractile profiles through a distinct mechanism independent of sarcolemmal damage.

To assess the effect of SOM treatment on the fatigue-like phenotypes resulting from the induction of sarcolemmal damage in DMD 3D tissues, we evaluated the contractile dynamics before and 24 h after the damage induction (figure 5(b)). Before damage induction, DMD tissues treated with SOM small molecule exerted, although non-significantly, higher twitch force (figure 5(c)). Moreover, they exhibited higher tetanic force (figure 5(d)). However, these forces were decreased after 24 h of the induction of the sarcolemmal damage and cessation of the treatment. In the context of tetanic contractions, we did not observe the appearance of fatigue-like tetanic dynamics after the control treatment of DMD tissues with DMSO or the SOM utrophin upregulator (figures 5(f) and (i)). Moreover, the increase of TIP and T75% after treatment with both DMSO and SOM was diminished, although not significantly, 24 h post-induction of damage (figures 5(h) and (j)). The absence of tetanic-like phenotypes in DMSO-treated tissues, as previously observed in DMD tissues, may be attributed to the influence of DMSO on membrane permeability and the resulting ion influx [41, 42], which could impact the contractile response of 3D skeletal muscle tissues to EPS. This effect is diminished after the removal of DMSO. Moreover, these results suggest that the efficacy of SOM utrophin upregulation treatment relied on its uninterrupted administration, as removing the treatment resulted in

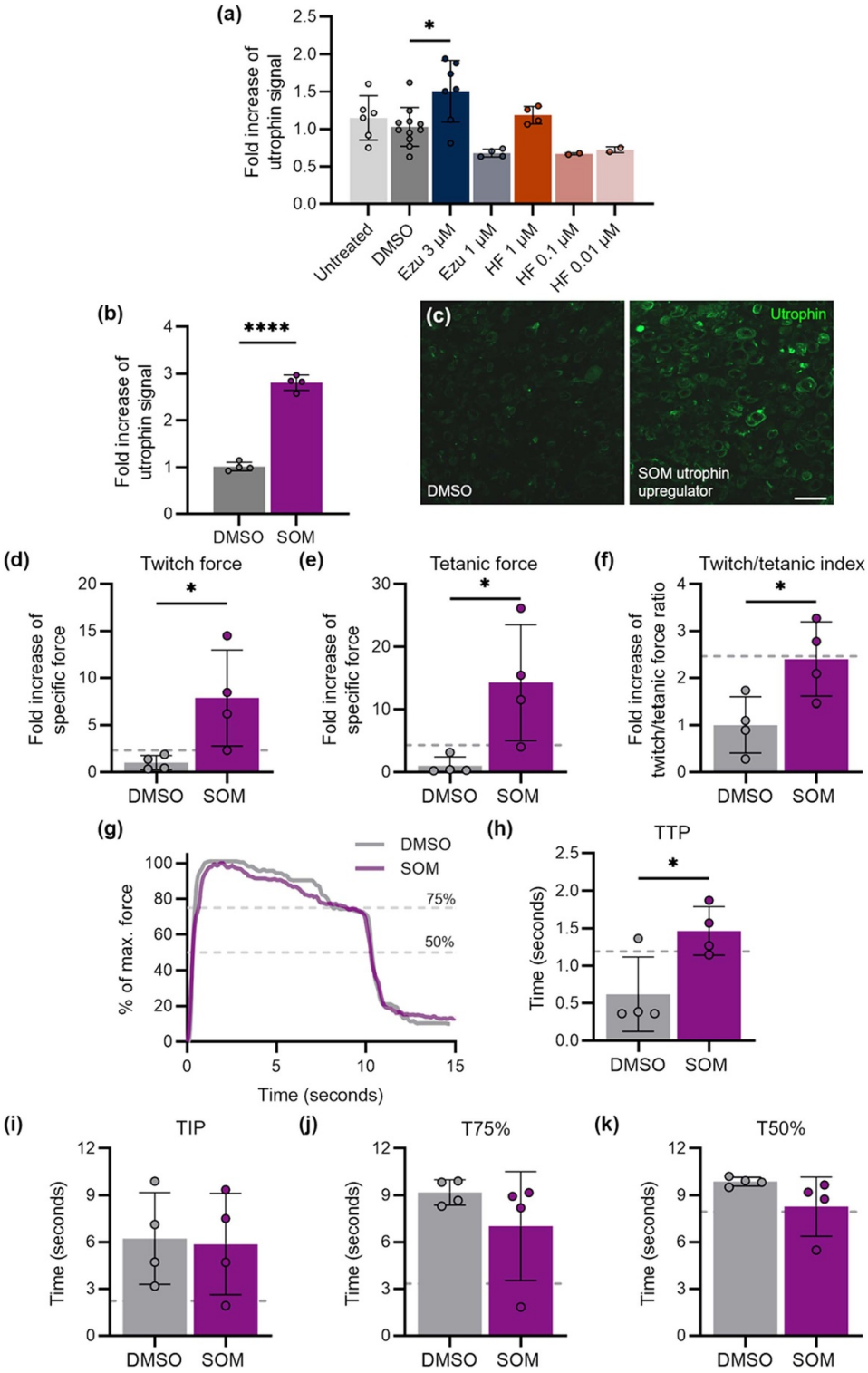

Figure 4. SOM utrophin upregulator improves DMD 3D skeletal muscle tissues functional performance. (a) and (b) Comparison of utrophin signal (expressed as the fold increase of the mean gray value of utrophin signal compared with values of tissues treated with dimethyl sulfoxide (DMSO) after 48 h treatment with 1–3 μM Ezutromid (Ezu), 0.01–1 μM Halofuginone (HF) (a) or 10 μM SOM utrophin upregulator (b). Datapoints represent mean values obtained from at least four utrophin confocal images. $N = 2$–6 tissues per group. (c) Representative confocal images of transversal cross-sections of DMD2 3D human skeletal muscle tissues after 48 h treatment with 10 μM SOM utrophin upregulator, stained for utrophin (green). (d)–(f) Fold increase of maximum twitch (d) and tetanic (e) specific forces and twitch/tetanic force ratio (f) compared with DMSO control performed by DMD2 tissues during 1 and 50 Hz stimulation after 48 h treatment with 10 μM SOM utrophin upregulator. (g) Representative force during 50 Hz stimulation for 10 s normalized to the maximum peak force performed by DMD2 tissues after 48 h treatment with 10 μM SOM utrophin upregulator or DMSO during 50 Hz stimulation for 10 s EPS. (h)–(k) Time to peak (h), time in peak (i) and time to relaxation to the 75% (j) and 50% (k) of the maximum force performed by DMD2 tissues after 48 h treatment with 10 μM SOM utrophin upregulator or DMSO during 50 Hz stimulation for 10 s EPS. Gray dashed lines indicate mean values performed by CNT2. $N = 4$ tissues per group. Significance was determined using one-way ANOVA followed by Tukey's range multiple comparisons test (a) and two-tailed student t-test (b)–(k) to compare differences between the groups. Statistical test outcomes are reported as mean ± SEM ($*p < 0.05$).

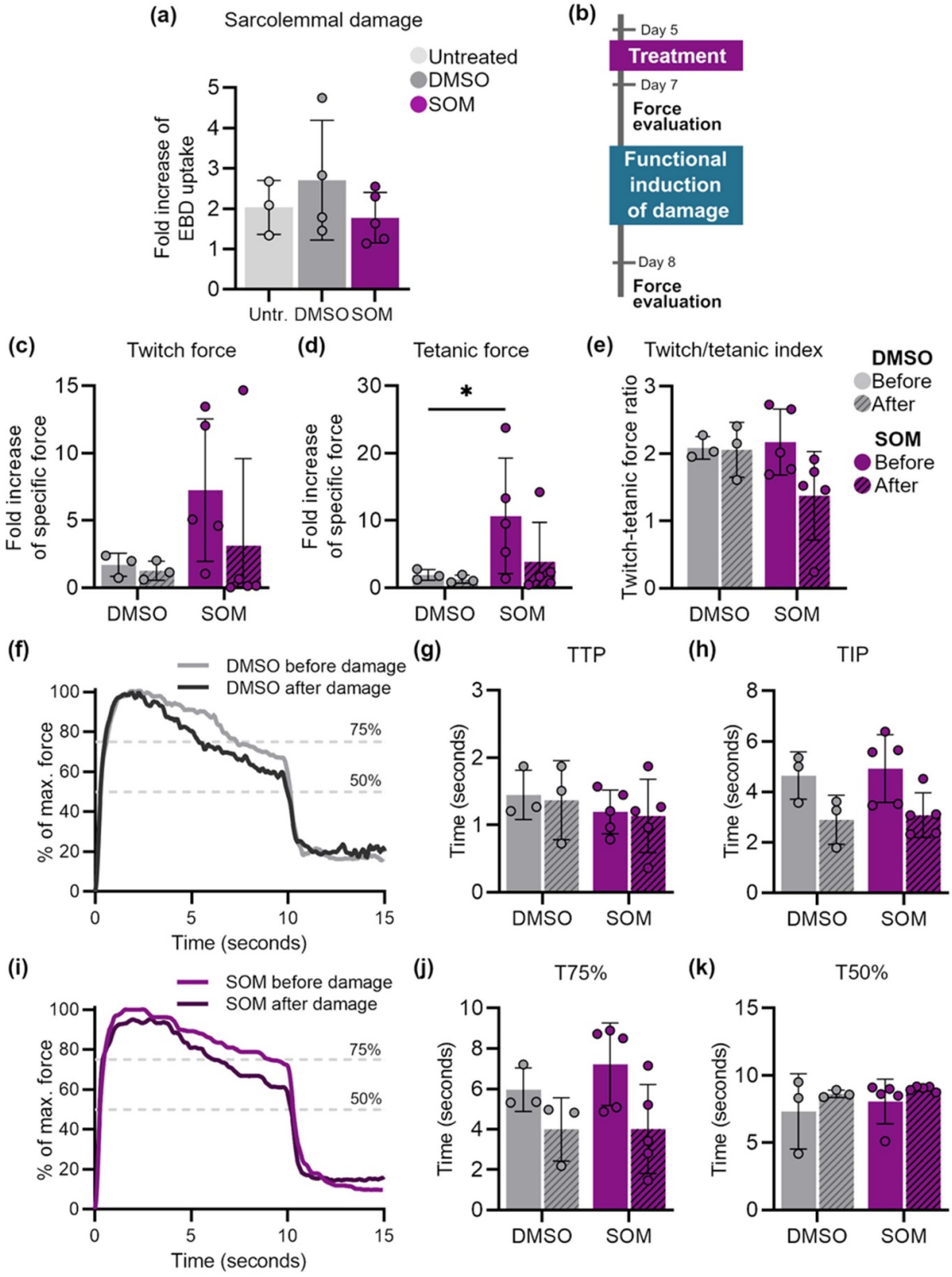

Figure 5. Sarcolemmal damage induction after treatment with SOM utrophin upregulator (a) comparison of Evans blue dye (EBD) uptake (expressed as the fold increase of the mean gray value of EBD per myotube compared with non-stimulated CNT2 levels and normalized using mean values of untreated tissues with data showed in figure 3(a)) of DMD2 tissues after 15 min of 1 Hz EPS. Datapoints represent mean values obtained from at least four EBD confocal images. $N = 3$–5 tissues per group. (b) Schematic of the experimental flow of the recovering of functional induction of damage. (c)–(e) Fold increase of maximum twitch (d) and tetanic (e) specific forces and twitch/tetanic force ratio (f) compared with non-stimulated dimethyl sulfoxide (DMSO) treated DMD2 tissues performed by treated DMD2 tissues before or after 24 h of the damage EPS during 1 and 50 Hz stimulation. (f), (i) Representative force during 50 Hz stimulation for 10 s normalized to the maximum peak force performed by DMD2 tissues treated with DMSO (f) or SOM utrophin upregulator (i) before or after 24 h of the damage EPS. (g)–(h), (j)–(k) time to peak (g), time in peak (h) and time to relaxation to the 75% (j) and 50% (k)) of the maximum force performed by DMD2 tissues treated with DMSO or SOM utrophin upregulator before or after 24 h of the damage EPS during 50 Hz stimulation for 10 s. $N = 3$–5 tissues per group. Significance was determined using one-way (a) or two-way repeated measures (c)–(k) ANOVA followed by Tukey's range multiple comparisons test to compare differences between the groups. Statistical test outcomes are reported as mean ± SEM ($*p < 0.05$).

the cessation of its effects on the 3D skeletal muscle tissues.

4. Discussion and conclusions

Over the last few years, there has been an increase in the development of many therapeutic approaches to treat DMD. However, most candidates developed thus far have failed to meet satisfactory endpoints in clinical stages [15], which reveals the presence of challenges impeding the success of promising DMD treatment candidates. This phenomenon can be attributed to various factors, but the inherent limitations of current preclinical DMD models play a substantial role. On the one hand, DMD *in vitro* skeletal muscle models are a valuable tool for assessing certain muscle-specific improvements, but they cannot reproduce some relevant physiological responses [43]. On the other hand, animal models present fundamental challenges. The *mdx* mouse, although commonly used, does not accurately replicate the human disease [44], and dystrophin-deficient dogs exhibit low efficiency, and their use is expensive and time-consuming [45]. Altogether, these limitations hinder the discovery and development of novel treatments to mitigate the progression of DMD.

Bioengineered 3D skeletal muscle models have emerged as a promising tool to complement and accelerate preclinical studies [25]. This technology enables the generation of functional skeletal muscle tissues that exhibit contractile activity, which can be monitored. This allows the reproduction of disease phenotypes that cannot be mimicked in 2D *in vitro* platforms. In this work, we generated a bioengineered 3D skeletal muscle for DMD that recapitulates the most characteristic early feature of dystrophin deficiency in DMD patients: the presence of sarcolemmal damage. We cultured immortalized muscle precursor cells [30] derived from three healthy donors and three DMD patients in a fibrin-composite matrix on a PDMS mold that contained two posts. These exerted tension on the material and, after seven days of differentiation, we observed differentiated myotubes that were aligned in the perpendicular axis to the posts of the mold (figures 1, S1 and S2).

All samples were competent to produce contractions in response to electrical stimulation, and we evaluated the functional performances that the skeletal muscle tissues showed during twitch and tetanic contractions (figure 2). None of the investigated parameters revealed disease-specific functional phenotypes, partly due to the variable responses to EPS among the cell lines. These results are consistent with the significant inter-individual variability that has been reported in the physiological responses to muscle contraction [46, 47], along with the inherent heterogeneity of DMD patients [48].

Next, we hypothesized that DMD tissues might perform differences only after the sarcolemma damage, which occurs due to the impact of mechanical forces generated during contractile activity on the unstable membrane of DMD myotubes [49, 50]. Considering this, we explored the impact of long twitch contraction cycles on sarcolemmal integrity in the CNT and DMD cell lines that presented the most interesting characteristics. Following this strategy, our DMD skeletal muscle model successfully reproduced sarcolemmal damage associated with DMD, revealing a functional phenotype characterized by muscle fatigue during tetanic contractions (figure 3). This represents a significant milestone as it provides an opportunity to explore the replication of additional manifestations of DMD stemming from a sarcolemmal injury, thereby initiating cellular degeneration and eventual muscle wasting [51].

To explore the model's ability to assess drug responses, we evaluate the impact of utrophin upregulators in DMD skeletal muscle tissues. First, we examined the small molecules Ezutromid and Halofuginone, previously suggested as utrophin upregulators [20, 21]. We only observed significant increases in utrophin levels after administering high concentrations of Ezutromid, which resulted in the loss of contractile response (figure 4).

We proceeded to evaluate the efficacy of a utrophin upregulator candidate, initially identified through *in silico* analysis conducted by SOM Innovation Biotech S.A. This finding was experimentally validated using our 3D DMD model (figure 4), as we observed nearly a three-fold increase in utrophin signaling. After the treatment, DMD tissues improved their functional performance, with some parameters reaching similar values to those of CNT samples. However, this improvement in the functional outcomes did not imply protection on the sarcolemmal damage (figure 5). These results suggested that utrophin upregulation did not entail the stabilization of the sarcolemma, which offers insight into the impact that the treatment may have on more advanced preclinical studies or even clinical phases. Furthermore, the absence of tetanic-like phenotypes in DMSO-treated tissues, holds significant interest due to the widespread use of DMSO in research and emphasize the importance of considering DMSO's potential influence.

Altogether, these findings underscore the potential of our DMD model to serve as a platform to gain a deeper understanding of how potential drugs and other molecules can influence skeletal muscle functionality. Notably, the outcomes from this 3D human DMD model suggest that both Ezutromid and Halofuginone may not be optimal candidates that target the increase of utrophin levels. Interestingly, these findings align with the results

from phase 2 trials involving these molecules, where the primary and secondary endpoints to assess their efficacy were not achieve (NCT02858362, NCT02525302, NCT01978366). This highlights how the incorporation of advanced 3D functional models into preclinical studies could provide predictive insights into therapeutic responses in subsequent stages.

To the best of our knowledge, this work reports the first functional bioengineered 3D skeletal muscle model of DMD that recapitulates sarcolemmal damage. By mimicking the pathophysiological rupture of the muscle membrane through replicating repeated contraction and relaxation cycles, this model improves the current state-of-the-art dystrophic 3D cell culture tools. Recent studies have described 3D DMD models using different patient-derived cell types, including primary [52] and immortalized [53] myoblasts or induced pluripotent stem cells (iPSCs) [54, 55], as well as isogenic diseased cell lines from healthy iPSCs and differentiated to myoblasts [56] or cardiomyocytes [57]. While some studies did not focus on the contractile activity in response to EPS [54], others conducted an electrophysiological analysis [58] or identified *de novo* dystrophin revertant fibers but were not able to detect sarcolemmal damage [53]. Functional DMD phenotypes have been reported in various studies, including contractile weaknesses [52], contractile and calcium transient defects [57], reduced twitch tension and prolonged contraction and relaxation times [55], as well as lower forces and contractile velocities [56]. However, the DMD 3D model developed in this work showcased the ability to not only functionally induce sarcolemmal damage but also to predict the response of potential DMD therapeutic drugs. Altogether, our DMD patient-derived 3D skeletal muscle model offers a relevant alternative to existing *in vitro* models, holding potential as a preclinical platform in future DMD drug developments.

The recent advances in 3D biofabrication methods, as well as the refinement of cell sources and cell culture techniques, will promote the increase of the complexity of 3D skeletal muscle models for DMD and other muscular dystrophies. This will allow the mimicking of complex pathophysiological events, including processes that involve more several cell types, such as fibrosis or inflammation [59]. This is crucial to obtain relevant outcomes and accurately predict the clinical response of a drug. Such advancements will develop relevant and versatile *in vitro* tools, which hold great promise to improve and accelerate the drug development processes.

Data availability statement

All data that support the findings of this study are included within the article (and any supplementary files).

Acknowledgments

We gratefully acknowledge SOM Innovation Biotech S A, Barcelona, Spain, for providing utrophin upregulator molecules, and Dr Bénédicte Chazaud from the Institut NeuroMyoGène (INMG), Lyon, France, for providing the human immortalized muscle precursor cells used in this study. We would like to express our appreciation to MicroFabSpace and Microscopy Characterization Facility, Unit 7 of ICTS 'NANBIOSIS' from CIBER-BBN at IBEC for their technical support. We extend our gratitude to the muscle team from the Biosensors for Bioengineering group for their valuable feedback during the review process of this manuscript. This work received financial support from Duchenne Parent Project Spain, Grant ID: DPPE/09_2020 (JMF-C), and the UK Research and Innovation (UKRI) from Medical Research Council (MRC), Grant ID: MR/WR019086/1 (JMF-C). AT-V was supported by a predoctoral fellowship (2022FI_B 00386) from Generalitat de Catalunya.

Author contributions

A T-V, M M, J R-A, and J M F-C collectively conceived the study and its objectives. A T-V and J M F-C carried out the experimental work and coordinated the data analysis. J M F-C secured the necessary funding for the project. A T-V took the lead in preparing the manuscript, with supervision from J M F-C, and incorporated input from all the authors.

Ethical statement

The authors declared no potential conflicts of interest with respect to the research, authorship, and/or publication of this article.

ORCID iDs

Ainoa Tejedera-Villafranca https://orcid.org/0000-0002-1897-073X
Javier Ramón-Azcón https://orcid.org/0000-0002-3636-8013
Juan M Fernández-Costa https://orcid.org/0000-0002-1854-6082

References

[1] Mah J K, Korngut L, Dykeman J, Day L, Pringsheim T and Jette N 2014 A systematic review and meta-analysis on the epidemiology of Duchenne and Becker muscular dystrophy *Neuromuscul. Disord.* **24** 482–91
[2] Bladen C L *et al* 2015 The TREAT-NMD DMD Global Database: analysis of more than 7,000 Duchenne muscular dystrophy mutations *Hum. Mutat.* **36** 395–402
[3] Duan D, Goemans N, Takeda S, Mercuri E and Aartsma-Rus A 2021 Duchenne muscular dystrophy *Nat. Rev. Dis. Primers* **7** 1–19

[4] Gao Q and McNally E M 2015 The dystrophin complex: structure, function and implications for therapy *Compr. Physiol.* **5** 1223–39

[5] Wallace G Q and McNally E M 2009 Mechanisms of muscle degeneration, regeneration, and repair in the muscular dystrophies *Annu. Rev. Physiol.* **71** 37–57

[6] Petrof B J 1998 The molecular basis of activity-induced muscle injury in Duchenne muscular dystrophy *Mol. Cell. Biochem.* **179** 111–23

[7] Rosenberg A S, Puig M, Nagaraju K, Hoffman E P, Villalta S A, Rao V A, Wakefield L M and Woodcock J 2015 Immune-mediated pathology in Duchenne muscular dystrophy *Sci. Transl. Med.* **7** 299rv4

[8] Passamano L *et al* 2012 Improvement of survival in Duchenne muscular dystrophy: retrospective analysis of 835 patients *Acta Myol.* **31** 121–5

[9] Dowden H and Munro J 2019 Trends in clinical success rates and therapeutic focus *Nat. Rev. Drug Discovery* **18** 495–6

[10] Iftikhar M, Frey J, Shohan M J, Malek S and Mousa S A 2021 Current and emerging therapies for Duchenne muscular dystrophy and spinal muscular atrophy *Pharmacol. Ther.* **220** 107719

[11] Crone M and Mah J K 2018 Current and emerging therapies for Duchenne muscular dystrophy *Curr. Treat. Options Neurol.* **20** 31

[12] Fortunato F, Rossi R, Falzarano M S and Ferlini A 2021 Innovative therapeutic approaches for Duchenne muscular dystrophy *J. Clin. Med.* **10** 820

[13] Goyenvalle A and Davies K E 2011 Challenges to oligonucleotides-based therapeutics for Duchenne muscular dystrophy *Skelet Muscle* **1** 8

[14] Aartsma-Rus A 2023 The future of exon skipping for Duchenne muscular dystrophy *Hum. Gene Ther.* **34** 372–8

[15] Lu Q, Cirak S and Partridge T 2014 What can we learn from clinical trials of exon skipping for DMD? *Mol. Ther.* **3** e152

[16] Fortunato F, Farnè M and Ferlini A 2021 The DMD gene and therapeutic approaches to restore dystrophin *Neuromuscul. Disorders* **31** 1013–20

[17] Reardon S 2023 'It's a vote for hope': first gene therapy for muscular dystrophy nears approval, but will it work? *Nature* **618** 451–3

[18] Soblechero-Martín P, López-Martínez A, de la Puente-ovejero L, Vallejo-Illarramendi A and Arechavala-Gomeza V 2021 Utrophin modulator drugs as potential therapies for Duchenne and Becker muscular dystrophies *Neuropathol. Appl. Neurobiol.* **47** 711–23

[19] Pines M and Nagler A 1998 Halofuginone: a novel antifibrotic therapy *Gen. Pharmacol. Vascular Syst.* **30** 445–50

[20] Mordechay S, Smullen S, Evans P, Genin O, Pines M and Halevy O 2021 Differential effects of halofuginone enantiomers on muscle fibrosis and histopathology in Duchenne muscular dystrophy *Int. J. Mol. Sci.* **22** 7063

[21] Levi O, Genin O, Angelini C, Halevy O and Pines M 2015 Inhibition of muscle fibrosis results in increases in both utrophin levels and the number of revertant myofibers in Duchenne muscular dystrophy *Oncotarget* **6** 23249–60

[22] Kapałczyńska M, Kolenda T, Przybyła W, Zajączkowska M, Teresiak A, Filas V, Ibbs M, Bliźniak R, Łuczewski Ł and Lamperska K 2018 2D and 3D cell cultures—a comparison of different types of cancer cell cultures *Arch. Med. Sci.* **14** 910–9

[23] Robinson N B *et al* 2019 The current state of animal models in research: a review *Int. J. Surg.* **72** 9–13

[24] Denayer T, Stöhr T and van Roy M 2014 Animal models in translational medicine: validation and prediction *New Horiz. Transl. Med.* **2** 5–11

[25] Fernández-Costa J M, Fernández-Garibay X, Velasco-Mallorquí F and Ramón-Azcón J 2021 Bioengineered *in vitro* skeletal muscles as new tools for muscular dystrophies preclinical studies *J. Tissue Eng.* **12** 204173142098133

[26] Ahadian S *et al* 2018 Organ-on-a-chip platforms: a convergence of advanced materials, cells, and microscale technologies *Adv. Healthcare Mater.* **7** 1700506

[27] Madden L, Juhas M, Kraus W E, Truskey G A and Bursac N 2015 Bioengineered human myobundles mimic clinical responses of skeletal muscle to drugs *eLife* **4** e04885

[28] Vesga-Castro C, Aldazabal J, Vallejo-Illarramendi A and Paredes J 2022 Contractile force assessment methods for *in vitro* skeletal muscle tissues *eLife* **11** e77204

[29] Moyle L A, Davoudi S and Gilbert P M 2022 Innovation in culture systems to study muscle complexity *Exp. Cell Res.* **411** 112966

[30] Massenet J, Gitiaux C, Magnan M, Cuvellier S, Hubas A, Nusbaum P, Dilworth F J, Desguerre I and Chazaud B 2020 Derivation and characterization of immortalized human muscle satellite cell clones from muscular dystrophy patients and healthy individuals *Cells* **9** 1780

[31] Fernández-Costa J M, Ortega M A, Rodríguez-Comas J, Lopez-Muñoz G, Yeste J, Mangas-Florencio L, Fernández-González M, Martin-Lasierra E, Tejedera-Villafranca A and Ramon-Azcon J 2022 Training-on-a-chip: a multi-organ device to study the effect of muscle exercise on insulin secretion *in vitro Adv. Mater. Technol.* **8** 2200873

[32] Schindelin J *et al* 2012 Fiji: an open-source platform for biological-image analysis *Nat. Methods* **9** 676–82

[33] Schneider C A, Rasband W S and Eliceiri K W 2012 NIH Image to ImageJ: 25 years of image analysis *Nat. Methods* **9** 671–5

[34] Mestre R, Patiño T, Barceló X, Anand S, Pérez-Jiménez A and Sánchez S 2019 Force modulation and adaptability of 3D-bioprinted biological actuators based on skeletal muscle tissue *Adv. Mater. Technol.* **4** 1800631

[35] Vijayaraghavareddy P, Adhinarayanreddy V, Vemanna R S, Sreeman S and Makarla U 2017 Quantification of membrane damage/cell death using Evan's blue staining technique *Bio-protocol* **7** e2519

[36] Pachitariu M and Stringer C 2022 Cellpose 2.0: how to train your own model *Nat. Methods* **19** 1634–41

[37] Waisman A, Norris A M, Elías Costa M and Kopinke D 2021 Automatic and unbiased segmentation and quantification of myofibers in skeletal muscle *Sci. Rep.* **11** 11793

[38] Yao L, Xue X, Yu P, Ni Y and Chen F 2018 Evans blue dye: a revisit of its applications in biomedicine *Contrast Media Mol. Imaging* **2018** e7628037

[39] Hamer P W, McGeachie J M, Davies M J and Grounds M D 2002 Evans blue dye as an *in vivo* marker of myofibre damage: optimising parameters for detecting initial myofibre membrane permeability *J. Anat.* **200** 69–79

[40] Chancellor D R *et al* 2011 Discovery of 2-arylbenzoxazoles as upregulators of utrophin production for the treatment of Duchenne muscular dystrophy *J. Med. Chem.* **54** 3241–50

[41] Gironi B, Kahveci Z, McGill B, Lechner B-D, Pagliara S, Metz J, Morresi A, Palombo F, Sassi P and Petrov P G 2020 Effect of DMSO on the mechanical and structural properties of model and biological membranes *Biophys. J.* **119** 274–86

[42] He F, Liu W, Zheng S, Zhou L, Ye B and Qi Z 2012 Ion transport through dimethyl sulfoxide (DMSO) induced transient water pores in cell membranes *Mol. Membr. Biol.* **29** 107–13

[43] Piga D, Salani S, Magri F, Brusa R, Mauri E, Comi G P, Bresolin N and Corti S 2019 Human induced pluripotent stem cell models for the study and treatment of Duchenne and Becker muscular dystrophies *Ther. Adv. Neurol. Disord.* **12** 1756286419833478

[44] Swiderski K and Lynch G S 2021 Murine models of Duchenne muscular dystrophy: is there a best model? *Am. J. Physiol. Cell Physiol.* **321** C409–12

[45] McGreevy J W, Hakim C H, McIntosh M A and Duan D 2015 Animal models of Duchenne muscular dystrophy: from basic mechanisms to gene therapy *Dis. Models Mech.* **8** 195–213

[46] Towse T F, Elder C P, Bush E C, Klockenkemper S W, Bullock J T, Dortch R D and Damon B M 2016 Post-contractile BOLD contrast in skeletal muscle at 7 T reveals inter-individual heterogeneity in the physiological responses to muscle contraction *NMR Biomed.* **29** 1720–8
[47] van Vossel K, Hardeel J, van de Casteele F, van der Stede T, Weyns A, Boone J, Blemker S S, Lievens E and Derave W 2023 Can muscle typology explain the inter-individual variability in resistance training adaptations? *J. Physiol.* **601** 2307–27
[48] Desguerre I, Christov C, Mayer M, Zeller R, Becane H-M, Bastuji-Garin S, Leturcq F, Chiron C, Chelly J and Gherardi R K 2009 Clinical heterogeneity of Duchenne muscular dystrophy (DMD): definition of sub-phenotypes and predictive criteria by long-term follow-up *PLoS One* **4** e4347
[49] Lovering R M and de Deyne P G 2004 Contractile function, sarcolemma integrity, and the loss of dystrophin after skeletal muscle eccentric contraction-induced injury *Am. J. Physiol. Cell Physiol.* **286** C230–8
[50] Lynch G S, Rafael J A, Chamberlain J S and Faulkner J A 2000 Contraction-induced injury to single permeabilized muscle fibers from mdx, transgenic mdx, and control mice *Am. J. Physiol. Cell Physiol.* **279** C1290–4
[51] Bencze M 2023 Mechanisms of myofibre death in muscular dystrophies: the emergence of the regulated forms of necrosis in myology *Int. J. Mol. Sci.* **24** 362
[52] Nesmith A P, Wagner M A, Pasqualini F S, O'Connor B B, Pincus M J, August P R and Parker K K 2016 A human *in vitro* model of Duchenne muscular dystrophy muscle formation and contractility *J. Cell Biol.* **215** 47–56
[53] Ebrahimi M *et al* 2021 De novo revertant fiber formation and therapy testing in a 3D culture model of Duchenne muscular dystrophy skeletal muscle *Acta Biomater.* **132** 227–44
[54] Maffioletti S M *et al* 2018 Three-dimensional human iPSC-derived artificial skeletal muscles model muscular dystrophies and enable multilineage tissue engineering *Cell Rep.* **23** 899–908
[55] Shahriyari M *et al* 2022 Engineered skeletal muscle recapitulates human muscle development, regeneration and dystrophy *J. Cachexia Sarcopenia Muscle* **13** 3106–21
[56] Smith A S *et al* 2022 High-throughput, real-time monitoring of engineered skeletal muscle function using magnetic sensing *J. Tissue Eng.* **13** 20417314221122130
[57] Bremner S B, Mandrycky C J, Leonard A, Padgett R M, Levinson A R, Rehn E S, Pioner J M, Sniadecki N J and Mack D L 2022 Full-length dystrophin deficiency leads to contractile and calcium transient defects in human engineered heart tissues *J. Tissue Eng.* **13** 20417314221119628
[58] Nguyen C T, Ebrahimi M, Gilbert P M and Stewart B A 2021 Electrophysiological analysis of healthy and dystrophic 3D bioengineered skeletal muscle tissues *Am. J. Physiol. Cell Physiol.* **321** C749–59
[59] Fernández-Costa J M, Tejedera-Villafranca A, Fernández-Garibay X and Ramón-Azcón J 2023 Muscle-on-a-chip devices: a new era for *in vitro* modelling of muscular dystrophies *Dis. Models Mech.* **16** dmm050107